

High-throughput screening of piezo-photocatalytic materials for hydrogen production

Zhao Liu,^{1,2} Biao Wang,^{1,2} Dewei Chu,³ and Claudio Cazorla⁴

¹*School of Materials Science and Engineering, Dongguan University of Technology, Dongguan 523808, China*

²*Research Institute of Interdisciplinary Science, Dongguan University of Technology, Dongguan 523808, China*

³*School of Materials Science and Engineering, UNSW Sydney, Sydney, NSW 2052, Australia*

⁴*Departament de Física, Universitat Politècnica de Catalunya, Campus Nord B4-B5, Barcelona E-08034, Spain*

Finding cost-effective and efficient photocatalytic materials able to catalyse the water splitting reaction under visible light is one of the greatest challenges in current environmental material science. Despite that many photocatalysts are already known in the context of green hydrogen production, strategies to systematically and rationally modify their optoelectronic properties to achieve desired photocatalytic performance are yet to be established. Piezoelectric materials react to mechanical stimuli by adjusting their band gaps and band alignments, thus offering a possible route to precise photocatalyst design. However, piezo-photocatalysts are relatively scarce and have been seldom investigated to date. Here, we present a high-throughput screening of piezo-photocatalytic materials performed over $\sim 1,000$ bulk piezoelectrics that relies on a simple electrostatic model and first-principles calculations. A total of ~ 10 previously overlooked binary and tertiary bulk compounds are theoretically identified as highly promising piezo-photocatalysts due to their appropriate optoelectronic properties and superb band alignment tunability driven by uniaxial strain.

About three quarters of the hydrogen consumed annually worldwide, currently around 70 million tonnes, are produced by methane reforming, which generates about 830 million tons of CO₂ emissions [1, 2]. Aimed at curbing carbon emissions and motivated by the increasingly reduced costs of renewable electricity, there is growing interest in producing hydrogen from water electrolysis. However, generating the global hydrogen demand entirely from electricity would require an electricity consumption of 3600 TWh, which is not efficient from an energy resources point of view (e.g., it surpasses the annual electricity production of the European Union). Finding alternative means to produce clean hydrogen is therefore critical for attaining sustainable energy and industry futures. In this context, photocatalytic hydrogen production via solar water splitting emerges as one of the most promising solutions.

Splitting water molecules into oxygen and hydrogen under visible light is possible with the assistance of photocatalytic materials [3, 4]. Efficient photocatalytic materials should fulfill a number of stringent physical conditions like (Fig.1a–b): (1) the energy band gap, E_g , should be larger than 1.23 eV but smaller than ≈ 3.0 eV

in order to be able to absorb the visible radiation from sunlight, (2) the bottom (top) of the conduction (valence) band, CBB (VBT), should be higher (lower) than the reduction (oxidation) potential H^+/H_2 (H_2O/O_2), HER (OER), which lies at -4.44 (-5.67) eV with respect to the vacuum level, and (3) the recombination rate of light-induced electron-hole charge carriers should be low. In addition to the above requirements, potential candidates should be also abundant and easy to synthesize. Therefore, finding suitable photocatalytic materials remains a challenging task.

Several chemical and nanostructuring approaches have been successful at improving the photocatalytic activity of archetypal inorganic compounds like TiO₂ and CeO₂ under sunlight [5–8]. However, the usual intricacy of nanostructuring methods along with the tremendous variability of the as-synthesized nanomaterials makes it difficult to identify general approaches for consistently enhancing the photocatalytic performance of crystals [9]. Consequently, progress in photocatalysis, and in particular in photocatalytic production of hydrogen, aided by rational design of materials remains limited [10].

Recently, some of us have shown by means of first-principles calculations that mechanical strains (biaxial and uniaxial) can modify the band-gap properties of transition-metal oxides in a significant and consistent manner [11, 12]. In practice, biaxial strains of 1–5% can be introduced in crystals by growing thin films on top of substrates that present a lattice mismatch [13, 14]. Similarly, uniaxial strains of comparable sizes can be realized in microstructured materials via mechanical actuation [15, 16] and/or exposure to ultrasound waves [17, 18]. Therefore, in view of the condition (1) above, mechanical stress in principle could be exploited to improve the photocatalytic activity of non-ideal materials by finely tuning their optoelectronic properties. However, achieving an adequate degree of predictability in the band-alignment variations of traditional semiconductors as induced by strain [see the condition (2) above] appears to be extremely challenging [11]. Such a lack of accomplishment critically hinders rational design of photocatalysts based on strain engineering.

Notwithstanding such limitations, a particular class of materials called piezoelectrics exhibit quantifiable and systematic band structure variations driven by mechanical stress. In response to a strain deformation, a finite electric field develops in the interior of piezoelectrics that (i) introduces an approximately linear variation of the energy bands throughout the crystal, and (ii) reduces

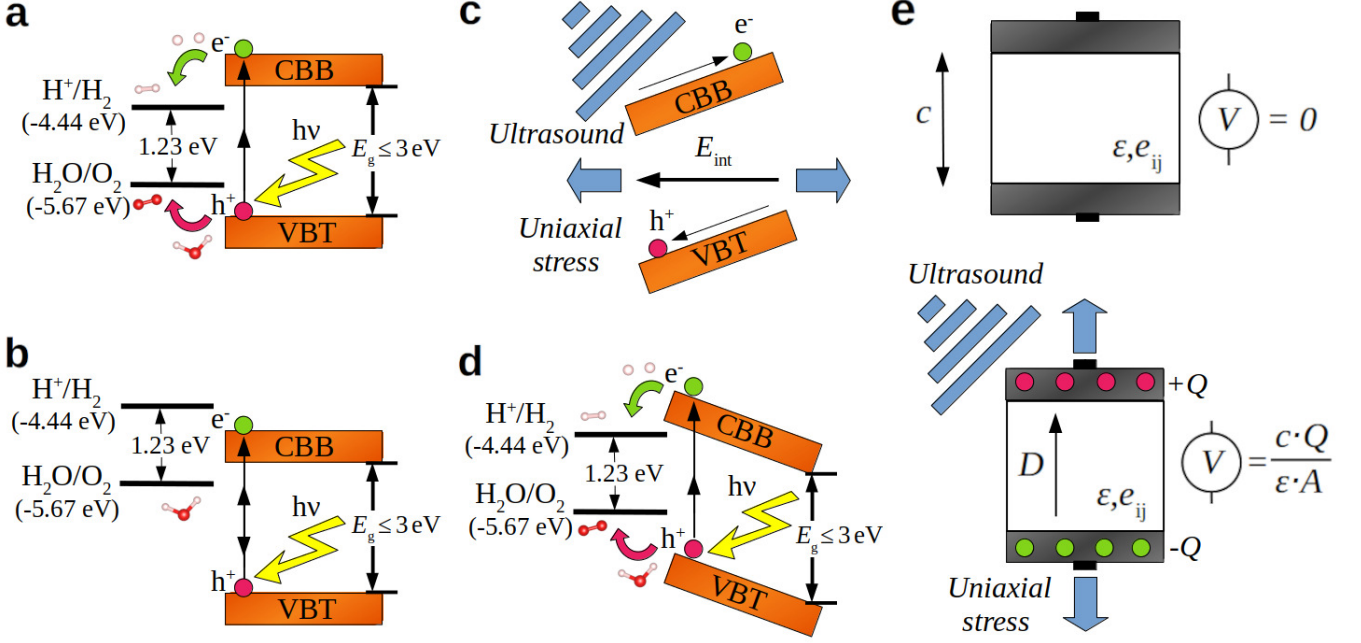


FIG. 1. Fundamental aspects of photocatalytic, piezoelectric and piezo-photocatalytic materials. **a** Opto-electronic properties of an ideal water-splitting photocatalyst; the conduction band bottom (CBB) and valence band top (VBT) of the photocatalyst perfectly straddle the OER and HER potentials as referred to the vacuum level. **b** Opto-electronic properties of a non-ideal water-splitting photocatalyst; the CBB and VBT of the photocatalyst fail to straddle the OER and HER potentials. **c** Application of uniaxial stress or ultrasound waves on a piezoelectric material induces an internal electric field and thus the appearance of a potential gradient. **d** Improvement of OER and HER straddling in a non-ideal photocatalyst that is piezoelectric achieved through uniaxial stress or ultrasound waves. **e** Simple parallel plate capacitor in which the dielectric material between the plates is a piezoelectric; upon application of uniaxial stress or ultrasound waves a finite voltage is created.

the recombination rate of migrating electron-hole pairs [see Fig.1c and conditions (2) and (3) above]. Moreover, piezoelectrics are non-centrosymmetric materials that encompass all pyroelectrics and ferroelectrics, hence they are abundant. These qualities are all very desirable for the rational engineering of novel materials with improved optoelectronic and photocatalytic properties (Fig.1d) [19] and some recent research have indeed focused on the study of archetypal “piezo-photocatalysts” like ZnO and BaTiO₃ [20–22]. Yet, a quantitative characterization and understanding of piezo-photocatalytic materials is lacking and the number of piezo-photocatalysts known to date is very limited.

In this work, we present a comprehensive first-principles computational study based on density functional theory (DFT) calculations that provides (i) a simple but physically insightful description of piezo-photocatalytic materials in terms of a piezoelectric plate capacitor (PPC) model, and (ii) a high-throughput screening of piezo-photocatalytic materials performed over a large database of $\sim 1,000$ bulk piezoelectrics [23] that relies on an easy-to-compute DFT descriptor. (Two-dimensional materials – e.g., g-C₃N₄ and GeS – and solid solutions – e.g., A_xA’_{1-x}B_yB’_{1-y}O₃ – are not included in the inspected database [23] hence despite of their photocatalytic promise such families of compounds

have been disregarded in the present study.) Based on our first-principles computational sieve, a number of previously overlooked binary and tertiary bulk compounds are identified as promising piezo-photocatalysts among which nitride (LaN and GaN), halide (PtF₄ and AgI), chalcogenide (BiTeCl, BiTeI and MgTe) and other inorganic (SiC) materials stand out due to their outstanding band-alignment tunability driven by uniaxial strain. Therefore, the present computational study has the potential to stimulate experimental synthesis of new piezo-photocatalytic materials able to boost the sustainable production of hydrogen based on solar water splitting.

RESULTS

In this section, a simple electrostatic model describing the band alignment rearrangements in a piezo-photocatalyst caused by uniaxial strain is first introduced along with an easy-to-compute first-principles descriptor of the resulting piezo-photocatalytic performance. Next, we present the main results of our high-throughput screening of piezo-photocatalytic materials performed over a large dataset of $\sim 1,000$ bulk piezoelectrics [23] followed by a careful quality check of the employed first-principles data. Finally, the outcomes

of our refined high-throughput screening are confronted with explicit calculations of the piezo-photocatalytic performance of one of the most promising identified compounds when subjected to broad uniaxial strain conditions. For the sake of focus, other relevant aspects to photocatalytic activity different from the materials electronic band structure properties (e.g., surface molecular reactions and light absorption processes) are left for future analysis.

Piezo-photocatalysts bulk modelling: The piezoelectric plate capacitor (PPC). To approximately model the band-alignment behavior of piezo-photocatalytic materials under stress, we start by examining the simple case of a parallel plate capacitor in which the dielectric material between the plates is piezoelectric (Fig.1e). Under open-circuit conditions and in the absence of mechanical stresses, the voltage drop among the plates of the capacitor, V , is null (we assume the spontaneous polarisation of the dielectric material to be zero). However, when a mechanical stress is applied on the capacitor V will be different from zero as a result of the accumulation of polarisation charges of different signs in the two capacitor plates. For the sake of simplicity, let us assume that (i) the mechanical stress (σ) is uniaxial and applied along the capacitor stacking direction, and (ii) the dielectric piezoelectric material is isotropic (Fig.1e). In such a case, the value of the potential drop can be evaluated as:

$$V = \frac{c \cdot Q}{\epsilon \cdot A} = \frac{c}{\epsilon} D, \quad (1)$$

where c represents the thickness of the capacitor, ϵ the dielectric constant of the piezoelectric material and D the charge per unit area accumulated in the plates. The value of the surface charge density can be determined via the isothermal piezoelectric stress constant of the dielectric material defined as:

$$e_{33} = \frac{\partial D}{\partial \eta}, \quad (2)$$

where $\eta \equiv \Delta c/c$ represents the stress-induced strain. Under small deformations it can be reasonably assumed that $D \approx e_{33}\eta$, hence the internal electric field that appears within the piezoelectric, E_{int} , can be also expressed in the linear approximation as:

$$E_{\text{int}}(\eta) = \frac{1}{c} V(\eta) = \frac{1}{c} \cdot \frac{\partial V}{\partial \eta} \eta \approx \frac{e_{33}}{\epsilon} \eta. \quad (3)$$

The following piezoelectric voltage coefficient can be defined from the formula above:

$$\alpha_\eta \equiv \frac{\partial V}{\partial \eta} = \frac{c}{\epsilon} e_{33}, \quad (4)$$

which describes the internal electrostatic potential variation induced by uniaxial strain. Based on the simple piezoelectric plate capacitor (PPC) model introduced

here, it can be reasonably argued that to a first approximation the maximum band-alignment change induced by uniaxial strain on a piezoelectric thin film is:

$$\Delta V_i(\eta) \equiv V_i(\eta) - V_i(0) = -c E_{\text{int}}(\eta) = -\alpha_\eta \eta, \quad (5)$$

where i stands for either the conduction band bottom (CBB) or valence band top (VBT) energy levels. (Here, surface dipoles are assumed to remain constant under small η 's.)

From Eq.(5), it is readily shown that piezoelectric materials presenting large (small) α_η coefficients [Eq.(4)] will offer great (poor) band-alignment tunability as driven by uniaxial strain. Consequently, piezoelectric materials possessing energy band gaps in the range of $1.23 \lesssim E_g \lesssim 3.0$ eV (to absorb the sunlight visible radiation), small dielectric constants and large piezoelectric stress coefficients (the last two conditions as for maximizing ΔV_i), *a priori* should be regarded as promising piezo-photocatalysts. It is noted that large piezoelectric stress constants typically are accompanied by also large dielectric constants [24, 25], thus the natural difficulty in finding materials with large band-alignment piezo tunability (i.e., large α_η values). This small set of conditions are not only physically insightful but also computationally convenient: the relevant quantities E_g , ϵ and e_{33} can be efficiently estimated via bulk first-principles DFT calculations [26–28]. As we will show in the next section, this circumstance can be exploited to conduct high-throughput computational searches of piezo-photocatalysts within large databases of piezoelectric materials that are publicly available [23].

It is important to note that the simple PPC model introduced here in principle should not be regarded as quantitatively accurate due to the involved simplifications (e.g., strain-induced E_g variations and surface dipole and surface relaxation effects have been neglected, and the assumed isotropic piezoelectric behaviour should not always be valid). Thus, any candidate piezo-photocatalyst identified on basis to the α_η descriptor should necessarily be put to test. In the next sections, we will comment on the extent of the possible limitations of the PPC model introduced in this section.

High-throughput piezo-photocatalysts screening. We performed a high-throughput computational search of piezo-photocatalysts over the Materials Project (MP) database containing about 1,000 different bulk piezoelectric compounds [23] (Methods). Figure 2 shows the steps followed in our high-throughput materials screening (Fig.2a) and the main results obtained from it (Fig.2b). Based on the PPC model introduced in the previous section and the DFT data available in the MP database, we applied two consecutive descriptor sieves on the reported bulk piezoelectrics. Compounds exhibiting a α_η coefficient larger than 1 eV [Eq.(4)] were first selected (which amounted to 42, Supplementary Table I) and from them those fulfilling the band-gap condition $1.23 \lesssim E_g \lesssim 3.0$ eV were finally retrieved. A total of 21

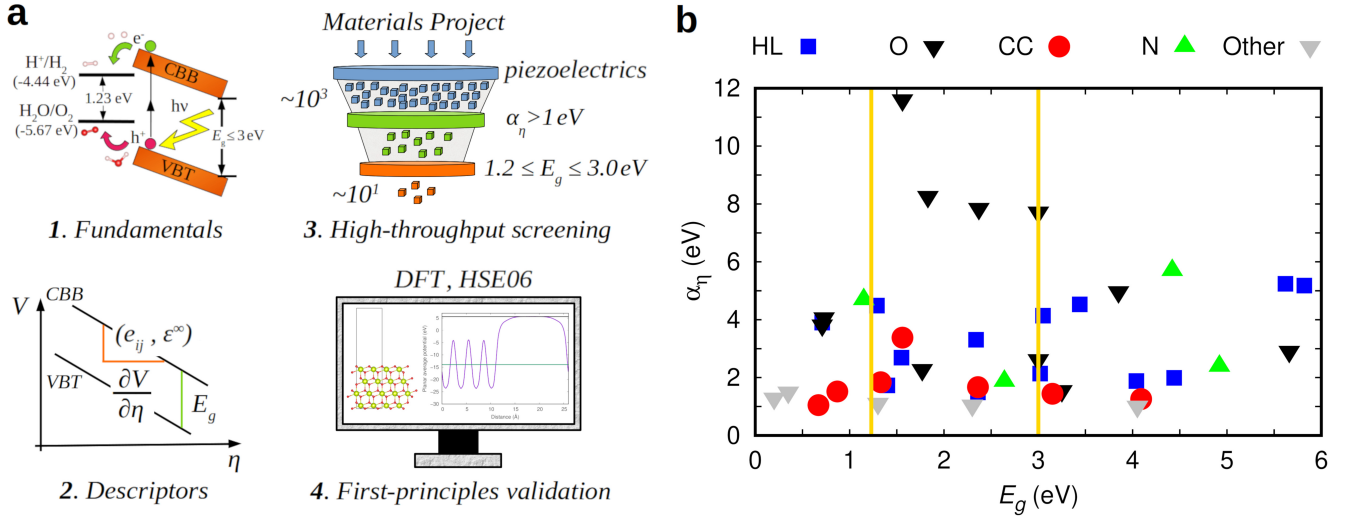


FIG. 2. High-throughput screening of piezo-photocatalytic materials for water splitting under visible light: strategy and results. **a** The adopted high-throughput screening strategy consists of a sequence of four steps. First, to understand the fundamentals of piezo-photocatalysts; second, to define a suitable set of easy-to-compute descriptors for piezo-photocatalytic materials; third, based on threshold descriptor values, to identify potential piezo-photocatalytic materials from the “Materials Project” database [23]; and fourth, to validate the results of the high-throughput screening by explicitly computing with first-principles methods the optoelectronic and band alignment properties of some of the identified piezo-photocatalysts. **b** High-throughput screening results. A total of 20 compounds were identified as potential piezo-photocatalytic materials for water splitting under visible light (Table I). The descriptor threshold values of $1.23 \lesssim E_g \lesssim 3.0$ eV are represented with gold vertical lines in the figure and only materials displaying $\alpha_\eta > 1$ eV are considered. “HL” stands for materials mostly containing halide atoms (F, Cl, Br, I), “O” oxygen atoms, “CC” chalcogenide atoms (S, Se, Te), “N” nitrogen atoms, and “Other” refers to inorganic compounds not classified in the previous categories.

compounds out of the initial $\sim 1,000$ piezoelectrics were tentatively identified as promising piezo-photocatalysts (Fig.2b), all of which are listed in Table I along with their most relevant properties.

Among the most promising piezo-photocatalysts we found some oxides (e.g., KNbO_3 , BaTiO_3 , NaNbO_3 and KIO_3), nitrides (e.g., LaN and $\text{Ge}_2\text{N}_2\text{O}$) and halides materials (e.g., PtF_4 , BaI_2 , BrF_3 and SeBr), most of which have not been previously investigated in the context of green hydrogen production. In terms of band-alignment tunability, non-centrosymmetric oxide perovskites (i.e., KNbO_3 , BaTiO_3 and NaNbO_3) emerge as the clear winners since they exhibit huge α_η values larger than or close to 10 eV. Several chalcogenides (e.g., BiTeCl and MgTe) and generic inorganic compounds (GaP and SiC) also were identified as potential photocatalysts, some of which appear to be especially promising in terms of reduced production costs (i.e., SiC).

It is worth noting that our first-principles based high-throughput search identified already well known piezo-photocatalysts like BaTiO_3 [20–22] and KNbO_3 [29, 30]. Other piezoelectric materials frequently employed in optoelectronic applications like ZnO and InN [31] were not retrieved by our computational analysis because the corresponding E_g values appearing in the MP database were noticeably smaller than 1.23 eV. For example, for hexagonal ZnO (space group $P6_3mc$ and MP identity number mp – 2133) we estimated a large α_η coefficient value of

4.07 eV, which turns out to be competitive with those of the top piezo-photocatalyst candidates listed in Table I; however, the ZnO band gap reported in the MP database amounts to 0.73 eV, which in principle would fail to properly straddle the OER and HER potentials [11] (see the Discussion section below).

Nonetheless, it is worth recalling here the inherent limitations of standard DFT approaches in estimating accurate band gaps in semiconductors due to the ubiquitous electronic self-interaction errors and other fundamental problems [32]. In particular, it is well known that common exchange-correlation functionals like LDA and GGA, which are computationally very affordable, tend to significantly underestimate E_g [34], and unfortunately (although also understandably) most of the results reported in the MP database are obtained with such standard DFT functionals. Thus, it is very likely that some of the candidate piezo-photocatalysts identified by our high-throughput search actually do not fulfill the band gap condition $E_g \lesssim 3.0$ eV. Similarly, it is also quite likely that some potentially good piezo-photocatalysts have escaped our computational sieve due to the systematic DFT underestimation of their band gap (e.g., hexagonal ZnO [11], see the Discussion section below). Furthermore, the reliability of the simple PPC model introduced in this work, upon which the present computational search has been built, needs to be checked. Consequently, we undertook a careful

assessment of the MP data and PPC model employed in our computational search by performing supplementary first-principles calculations.

First-principles data refinement. We re-evaluated the structural, dielectric, piezoelectric and band gap properties of the 21 compounds listed in Table I by using stringent convergence parameters and fairly accurate DFT functionals (Methods). Specifically, we re-optimized the relevant atomic geometries with a large energy cut-off of 800 eV and a \mathbf{k} -point grid of spacing $2\pi \times 0.01 \text{ \AA}^{-1}$ for sampling of the first-Brillouin zone, using the PBEsol exchange-correlation functional [33] (this DFT functional has been consistently ranked among the best performers in terms of lattice parameters prediction for semiconductors [35]). The dielectric, piezoelectric and band gap properties of the PBEsol-relaxed structures were subsequently estimated with the range-separated hybrid HSE06 potential [34]. By proceeding in this manner, an homogeneous and consistently high level of numerical accuracy was guaranteed for all the investigated materials.

Figure 3a shows a comparison of the band gaps found in the MP database, E_g , and those estimated by following the strategy explained above, E_g^{HSE06} , for all the materials reported in Table I. As it was expected, E_g^{HSE06} turns out to be significantly larger than E_g for most materials (discrepancies amount to 60–110% in the worse cases; see deviations from the solid black line in Fig.3a). Upon correction of the usual band-gap underestimation obtained with local and semi-local DFT methods, 7 out of the 21 initially selected potential piezo-photocatalysts were discarded because their E_g^{HSE06} 's were noticeably larger than 3 eV. The rejected materials were: NaNbO_3 , Na_2O_2 , BrF_3 , GeN_2O_2 , KNO_2 , BaI_2 and TlF (Fig.3a).

Likewise, Fig.3b shows a comparison of the piezoelectric voltage coefficients calculated with the DFT data found in the MP database, α_η , and the corresponding revised values estimated as explained above, α_η^{rev} , for all the materials reported in Table I. In this occasion, the consensus between the two sets of equivalent data is somewhat improved as compared to the band-gap case, although from a quantitative point of view their agreement is still far from satisfactory (in few instances the discrepancies are larger than 100%; see deviations from the solid black line in Fig.3b). Interestingly, we appreciate a quite systematic underestimation of α_η^{rev} obtained with local and semi-local DFT approaches, which for our present materials screening purposes does not represent a critical shortcoming (i.e., since we are interested in finding compounds with piezoelectric potential coefficients larger than a specific threshold value). Nevertheless, in the particular case of TlF and GaP we found that $\alpha_\eta^{\text{rev}} < 1 \text{ eV}$ hence they were discarded as potential piezo-photocatalysts (it is worth noting that upon refinement of the MP data only TlF failed to fulfill the two conditions guiding our computational searches).

As a result of our supplementary first-principles

calculations, a total of 8 out of the 21 initially identified candidate materials were rejected. The definitive set of potentially good piezo-photocatalysts is listed in Table II along with their re-evaluated E_g^{HSE06} and α_η^{rev} values. It is noted that few compounds exhibiting energy band gaps marginally larger than 3 eV were not discarded (i.e., GaN , MgTe and SiC) since our estimations may still contain small numerical imprecisions of the order of 0.1 eV [32]. There are appreciable quantitative differences among the two rankings of materials shown in Tables I and II that will be discussed in a subsequent section. Next, we turn our attention to the first-principles validation of the proposed PPC model and the computationally sieved piezo-photocatalytic materials.

First-principles validation of the PPC model and identified piezo-photocatalysts. For this crucial and computationally intensive part of our study, namely, explicit first-principles assessment of piezo-photocatalyst performances (i.e., not relying on materials descriptors) and testing of the PPC model, we selected SiC for several reasons. First, it is a very well-known and chemically simple material made of abundant and non-toxic elements that can be synthesised in a commercially large scale, hence from an applied point of view it is a very promising compound. Second, SiC exhibits several polymorphs some of which are piezoelectric (e.g., 2H and 4H) some of which are not (e.g., 3C), thus comparing their photocatalyst performances under uniaxial strain may result particularly meaningful. Third, despite of its high mechanical strength, several works in the literature have reported successful stabilisation of tensile uniaxial strains of $\approx 7 \%$ in nanostructured SiC [16], which is the maximum $|\eta|$ considered in the present work. And fourth, SiC appears in the last position of the lists enclosed in Tables I and II hence positive evaluation of this compound in principle may also suggest suitable piezo-photocatalyst performances for the rest of materials ranked above it.

Figure 4a shows the impact of uniaxial strain on the band gap of SiC considering the piezoelectric polymorph 4H (hexagonal, space group $P6_3mc$). Strain-induced band lifting effects are fully taken into consideration in our first-principles DFT results. In the absence of any stress, the E_g^{HSE06} of 4H- SiC is indirect (Fig.4b) and approximately amounts to 3.3 eV. (It is noted that the SiC band gap reported in Table II corresponds to the 2H polymorph, which is slightly smaller; for our validation analysis we have selected 4H- SiC because this is one of the most well-known and easy to synthesise silicon carbide polymorphs.) Under either tensile or compressive uniaxial strains, E_g^{HSE06} is significantly reduced and its indirect nature is conserved (Fig.4b). The maximum η -induced band-gap reduction is achieved in the compressive side, where appropriate photocatalytic values below 3 eV are obtained for uniaxial strains larger than $\approx 3\%$ (in absolute value). Meanwhile, in the tensile side the strain-induced E_g^{HSE06} variation is less regular and suit-

Formula	mp – ID	Space Group	c (Å)	ϵ (ϵ_0)	$ e_{33} $ (C · m ⁻²)	E_g (eV)	α_η (eV)	Type
KNbO ₃	4342	$P4mm$ (99)	4.09	12.98	3.26	1.56	11.6	O
BaTiO ₃	5986	$P4mm$ (99)	4.07	19.24	3.45	1.83	8.26	O
NaNbO ₃	4681	$Pmc2_1$ (26)	6.39	29.60	3.22	2.37	7.85	O
KIO ₃	552729	$R3m$ (160)	4.53	9.03	1.36	3.00	7.72	O
LaN	567290	$P6_3mc$ (186)	4.74	20.48	1.79	1.15	4.69	N
PtF ₄	8943	$Fdd2$ (43)	6.02	5.92	0.39	1.29	4.49	HL
BaI ₂	568536	$P\bar{6}2m$ (189)	7.94	14.52	0.67	3.05	4.14	HL
BiTeCl	28944	$P6_3mc$ (186)	7.58	4.57	0.18	1.56	3.38	CC
BrF ₃	23297	$Cmc2_1$ (36)	5.32	19.30	1.06	2.34	3.31	HL
SeBr	570589	$Aea2$ (41)	8.02	4.72	0.14	1.55	2.69	HL
KNO ₃	6920	$R3m$ (160)	4.44	4.22	0.22	3.00	2.62	O
Na ₂ O ₂	2340	$P\bar{6}2m$ (189)	5.69	5.36	0.19	1.77	2.28	O
TlF	558134	$Aem2$ (39)	4.67	48.33	1.96	3.02	2.14	HL
Ge ₂ N ₂ O	4187	$Cmc2_1$ (36)	5.42	8.18	0.25	2.64	1.87	N
BiTeI	22965	$P3m1$ (156)	5.41	6.67	0.20	1.33	1.84	CC
GaN	804	$P6_3mc$ (186)	3.89	11.65	0.46	1.74	1.75	N
AgI	22894	$P6_3mc$ (186)	5.68	7.43	0.20	1.40	1.73	HL
MgTe	1039	$P6_3mc$ (186)	5.58	8.31	0.22	2.36	1.67	CC
PI ₃	27529	$P6_3$ (173)	7.79	2.96	0.05	2.36	1.49	HL
GaP	8882	$P6_3mc$ (186)	4.72	13.02	0.27	1.30	1.11	Other
SiC	7140	$P6_3mc$ (186)	3.75	11.32	0.28	2.30	1.05	Other

TABLE I. Materials classified as potentially good piezo-photocatalysts for water splitting under visible light according to our first-principles high-throughput screening. Compounds are ranked according to their α_η value estimated with the DFT data retrieved from the Materials Project (MP) database. “mp-ID” stands for the compound identification number in the MP database [23], “HL” for halide materials, “O” for oxides, “CC” for chalcogenides, “N” for nitrides, and “Other” for inorganic compounds not classified in the previous categories.

Formula	Space Group	E_g^{HSE06} (eV)	α_η^{rev} (eV)	Drawbacks
KIO ₃	$R3m$ (160)	2.69	13.46	Water soluble
KNbO ₃	$P4mm$ (99)	2.44	10.81	–
LaN	$P6_3mc$ (186)	1.92	9.67	High cost
PtF ₄	$Fdd2$ (43)	2.67	8.80	High cost
BaTiO ₃	$P4mm$ (99)	2.95	8.03	–
SeBr	$Aea2$ (41)	1.34	7.00	Water soluble
PI ₃	$P6_3$ (173)	2.05	3.56	Water reacting
BiTeCl	$P6_3mc$ (186)	1.55	3.52	High cost
GaN	$P6_3mc$ (186)	3.09	3.35	High cost
MgTe	$P6_3mc$ (186)	3.02	2.22	High cost
AgI	$P6_3mc$ (186)	2.27	1.99	–
BiTeI	$P3m1$ (156)	1.45	1.96	High cost
SiC	$P6_3mc$ (186)	3.12	1.57	–

TABLE II. Revised list of potential piezo-photocatalysts for water splitting under visible light based on the refinement of the DFT data employed in our initial first-principles high-throughput screening. Compounds are ranked according to their revised piezoelectric voltage coefficient, α_η^{rev} . Potential practical drawbacks are indicated for each material.

able photocatalytic band-gap values are only attained at uniaxial distortions larger than $\approx 5\%$. We have checked that the vibrationally stability of the 4H-SiC polymorph is preserved upon application of the largest strains considered in this study (i.e., no imaginary lattice phonon bands appear in the two limit cases $\eta = \pm 7\%$, Fig.4c).

Figure 4d shows the variation of the 4H-SiC band alignments as induced by uniaxial strain (Methods). At zero strain, the VBT and CBB levels fail to correctly straddle the OER and HER potentials due to the existence of large negative offsets (e.g., the VBT level is approximately positioned 2 eV below the OER energy). When uniaxial strain is applied, however, the VBT and CBB levels are significantly displaced towards higher energies in the compressive side and towards lower energies in the tensile side. As a result, upon compressive uniaxial strains of $|\eta| > 4\%$ the band alignments of 4H-SiC are optimally positioned for straddling the OER and HER levels. It is also appreciated that the induced band-alignment changes can be regarded as roughly linear in η (at least locally). Therefore, based on our first-principles calculations, it is concluded that although unstrained 4H-SiC does not seem to be an optimal water-splitting photocatalyst its green hydrogen production performance can be substantially improved by means of compressive uniaxial strain (i.e., both the band gap and band alignments

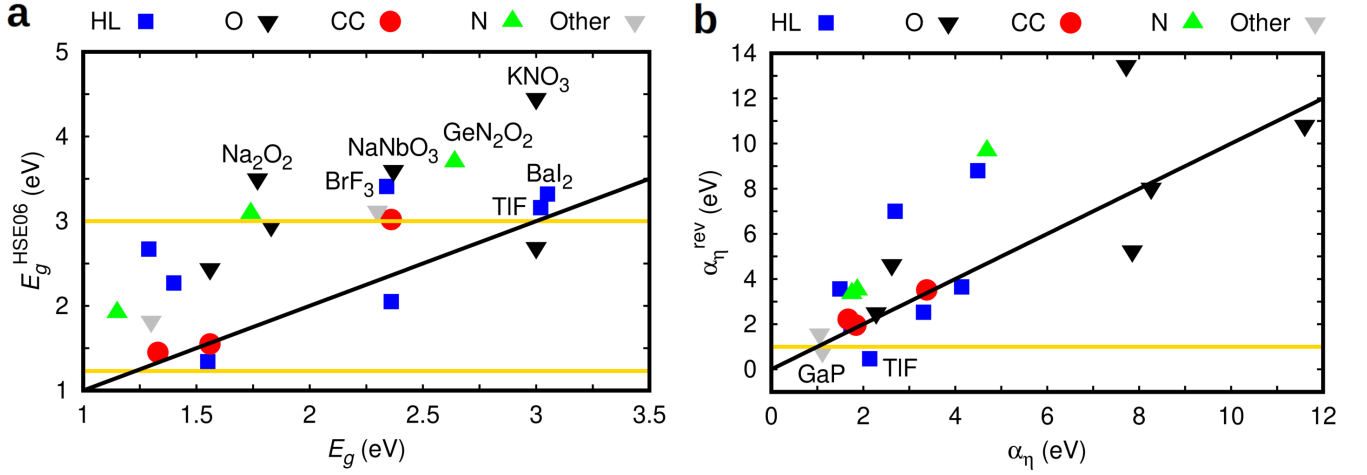


FIG. 3. Refinement of the first-principles data retrieved from the MP database. **a** MP band gap, E_g , versus HSE06 band gap, E_g^{HSE06} [34]. **b** Piezoelectric voltage coefficient calculated from the MP database, α_η , and from fully converged first-principles calculations based on the PBEsol [33] and HSE06 functionals, α_η^{rev} . As a result of our DFT data refinement, 7 out of the initially identified 20 potentially good piezo-photocatalysts for water splitting under visible light (Table I) were discarded (i.e., those named in the figures) since they did not fulfill either the condition of $1.23 \lesssim E_g^{\text{HSE06}} \lesssim 3.0$ eV and/or $1 < \alpha_\eta^{\text{rev}}$ (gold lines). The solid black lines with a slope equal to one are guides to the eye for better appreciating the $E_g - E_g^{\text{HSE06}}$ and $\alpha_\eta - \alpha_\eta^{\text{rev}}$ discrepancies.

can be appropriately tuned for such an end). Analogous band-alignment results are also obtained for the piezoelectric 2H-SiC polymorph (hexagonal, space group $P6_3mc$), although in this latter case straddling of the OER and HER levels is already attained in the absence of structural distortions (Supplementary Fig.1).

The outcomes obtained for 4H-SiC are encouraging and qualitatively consistent with the simple PPC model introduced above, that is, in agreement with the potential energy variation predicted by Eq.(5). At the quantitative level, however, the accordance between the computed α_η coefficients and the explicitly estimated first-principles $dV/d\eta$ variations are fair but not exact. For instance, by taking numerical derivatives on the VBT data represented in Fig.4d we obtain a η -induced potential variation of 29 (6), 18 (6) and 16 (6) eV for uniaxial strains of -7 , 0 and $+7\%$, respectively (numerical uncertainties are expressed within parentheses). Meanwhile, the physically equivalent α_η values calculated with Eq.(4) for the same lattice strains are 22, 1 and 23 eV, respectively (i.e., the structural, dielectric and piezoelectric parameters defining the α_η coefficient have been recalculated at each uniaxial strain). Clearly, the numerical agreement between the two sets of α_η data is not satisfactory although in the two limit $|\eta|$ cases, for which the e_{33} coefficient largely increases (and so does α_η), the accordance is significantly improved. Several straightforward reasons explaining the lack of quantitative precision of the PPC model are: (i) the neglect of η -induced band gap variations (i.e., the VBT and CBB levels are treated identically whereas in practice they may react slightly different to strain, as it is shown in Fig.4d); (ii) the assumption of a perfectly isotropic piezoelectric medium may be too

ideal (i.e., in practice, most piezoelectric tensors exhibit non-zero off-diagonal components hence the disregarded secondary lattice distortions may also accumulate charge along the principally strained direction, thus influencing the potential variation in the material); and (iii) the disregarding of surface dipole and surface relaxation effects.

It is worth commenting on the sign of the ΔV_i shift ($i = \text{VBT, CBB}$) as induced by η . In standard piezoelectrics, piezoelectric and piezoelectric voltage (Eq.4) coefficients are positively defined ($e_{33}, \alpha_\eta > 0$); thus, according to the PPC model, under tensile uniaxial strain ($\eta > 0$) the electrostatic potential in the interior of the material should rise as referred to the zero vacuum level (Eq.5 and Fig.1c). Conversely, under compressive uniaxial strain ($\eta < 0$) the electrostatic potential in the interior of the piezoelectric should come closer to the zero vacuum level (Eq.5). These ΔV_i trends predicted by the PPC model in fact are clearly reproduced by the DFT results enclosed in Fig.4d. Furthermore, we performed supplementary band alignment calculations for an anomalous piezoelectric material exhibiting negative piezoelectric and piezoelectric voltage coefficients ($e_{33}, \alpha_\eta < 0$). In this latter case, the expected η -induced ΔV_i shifts are opposite to those just explained, namely, tensile (compressive) uniaxial strain reduces (increases) the electrostatic potential in the interior of the material as referred to the zero vacuum level. Consistently, our DFT calculations reproduce the potential trends anticipated by Eq.(5) also in this case (Supplementary Fig.2).

Figure 5 shows equivalent results to those just explained for 4H-SiC but obtained for the non-piezoelectric polymorph 3C-SiC (cubic, space group $F43m$). The band gaps are also indirect in this case but noticeably

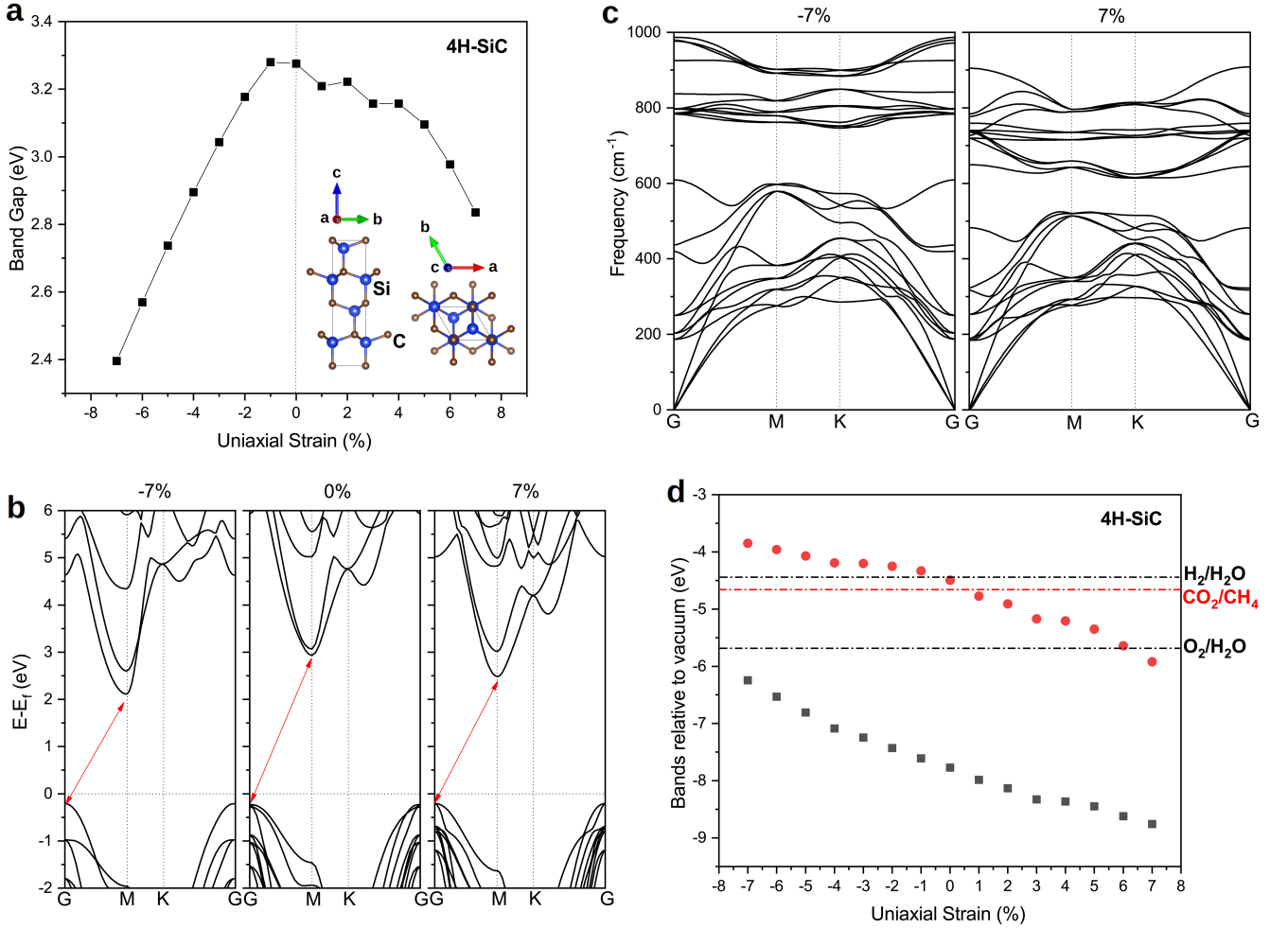


FIG. 4. First-principles analysis of the optoelectronic, vibrational, and band alignment properties of piezoelectric 4H-SiC. **a** Band-gap variation induced by uniaxial strain. **b** Dependence of the electronic band structure on uniaxial strain and reciprocal space point. **c** Phonon frequencies estimated as a function of uniaxial strain and reciprocal space point. **d** Effect of uniaxial strain on the band alignments of the crystal as referred to the vacuum level. The VBT and CBB energy levels are represented with solid grey squares and red circles, respectively.

smaller than estimated for 4H-SiC (Fig.5a,b). (Strain-induced band lifting effects are fully taken into consideration in our first-principles DFT results.) For instance, in the absence of strain E_g^{HSE06} amounts to 2.3 eV and at $\eta = -7\%$ to 1.3 eV. The η -induced band-gap variations in 3C-SiC resemble those calculated for 4H-SiC but they are more regular and somewhat larger. Likewise, the vibrational stability of the system is not affected by the lattice strain (Fig.5c). Nonetheless, the band alignments of non-piezoelectric 3C-SiH under strain behave radically different from those of piezoelectric 4H-SiC (Fig.5d). In particular, the induced VBT and CBB shifts are quite small (i.e., at most ≈ 0.5 eV) and not proportional to the applied strain (i.e., essentially they seem to follow the η -driven E_g^{HSE06} variations appearing in both compressive and tensile sides). Consequently, the water-splitting photocatalytic properties of non-piezoelectric 3C-SiC cannot be effectively tuned via uniaxial stress and the system re-

mains largely unsuitable for green hydrogen production (i.e., appropriate straddling of the OER and HER energy levels is never achieved through η).

Several general conclusions can be extracted from the results presented in this section. First, the band alignments of piezoelectric materials in fact can be tailored by uniaxial strain in a systematic and efficient manner. Second, the η -induced band-alignment changes predicted by the simple PPC model are physically well-motivated and thus can be used for the screening of potential piezophotocatalytic materials. (Furthermore, whenever the band alignments of an unstrained piezoelectric compound are known the simple PPC model can be used to roughly estimate the amount of tensile or compressive uniaxial strain that is needed to shift them towards optimal levels.) And third, the list of potential water-splitting piezophotocatalytic materials enclosed in Table II, although probably not exhaustive (see below), should be regarded

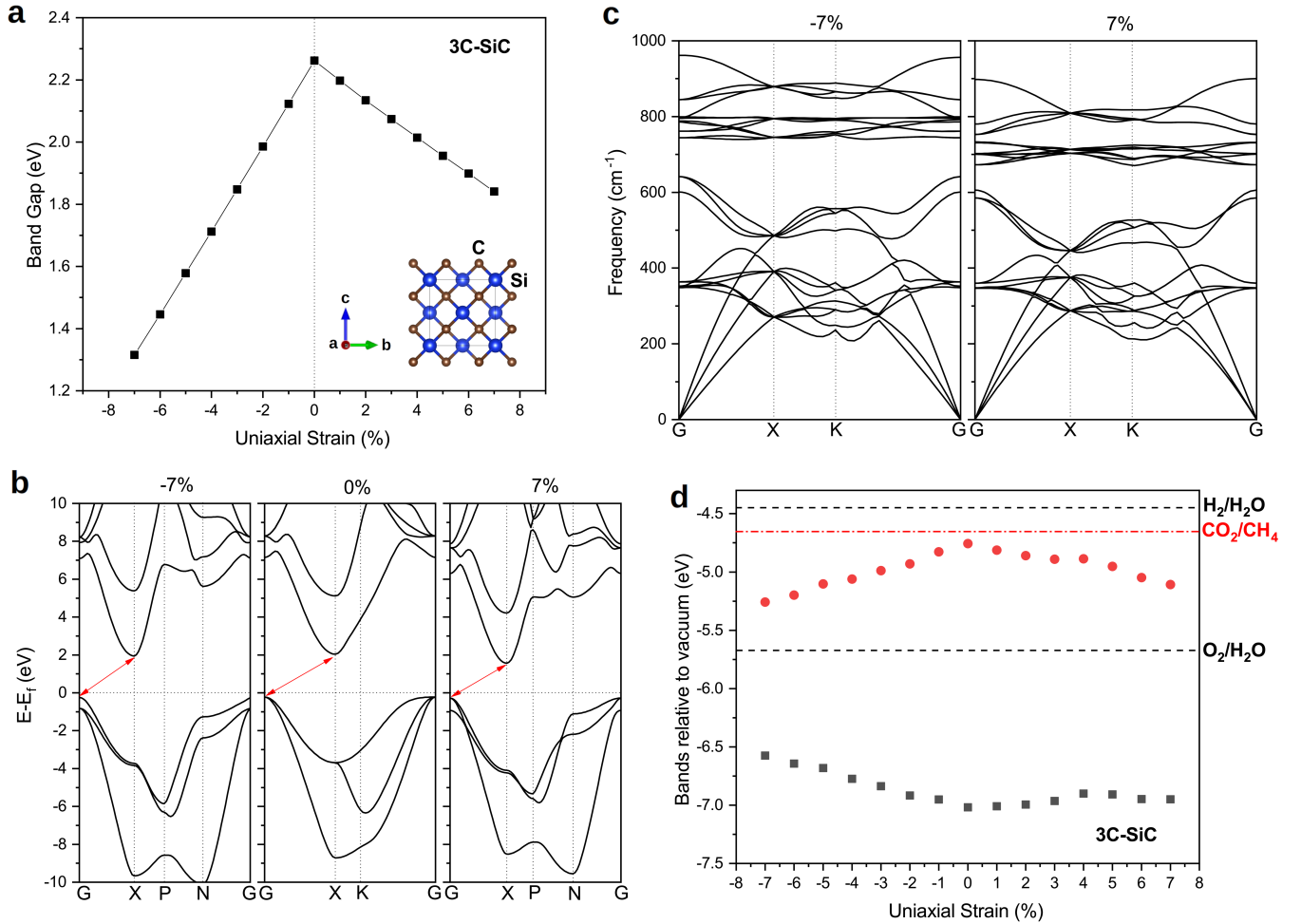


FIG. 5. First-principles analysis of the optoelectronic, vibrational, and band alignment properties of non-piezoelectric 3C-SiC. **a** Band-gap variation induced by uniaxial strain. **b** Dependence of the electronic band structure on uniaxial strain and reciprocal space point. **c** Phonon frequencies estimated as a function of uniaxial strain and reciprocal space point. **d** Effect of uniaxial strain on the band alignments of the crystal as referred to the vacuum level. The VBT and CBB energy levels are represented with solid grey squares and red circles, respectively.

as trustworthy and hence it may be key in guiding strain-assisted experiments in the field of green hydrogen production.

DISCUSSION

The two rankings of piezo-photocatalytic materials shown in Tables I and II, respectively deduced from the DFT data comprising the MP database and our refined DFT calculations, display appreciable quantitative differences. For instance, in Table I the value of the reported piezoelectric potential coefficients are typically smaller than in Table II and the top positions in the first list are predominantly occupied by oxide perovskites (whereas KIO_3 in the first position of Table II is an inorganic salt). Furthermore, upon refinement of the structural, piezoelectric and dielectric DFT data several ma-

terials initially classified as suitable water-splitting piezo-photocatalysts in Table I were finally discarded and not included in Table II (e.g., KNO_3 , GaP and TiF). On the other hand, at the qualitative level both materials rankings are generally equivalent since oxide, nitride and halide compounds are consistently presented as most promising. Therefore, for piezo-photocatalyst screening purposes the DFT data contained in the MP database should be regarded as of sufficient quality. For the rest of this section, however, we will concentrate our analysis on the materials reported in Table II.

The first of all ranked piezo-photocatalysts, KIO_3 , appears to be auspicious both in terms of band alignments tunability (i.e., largest $\alpha_{\eta}^{\text{rev}}$ value) and economical costs (i.e., all the integrating elements are abundant); however, this material is soluble in water and therefore is of little practical relevance in the context of water splitting photocatalysis. Similar water solubility and water reac-

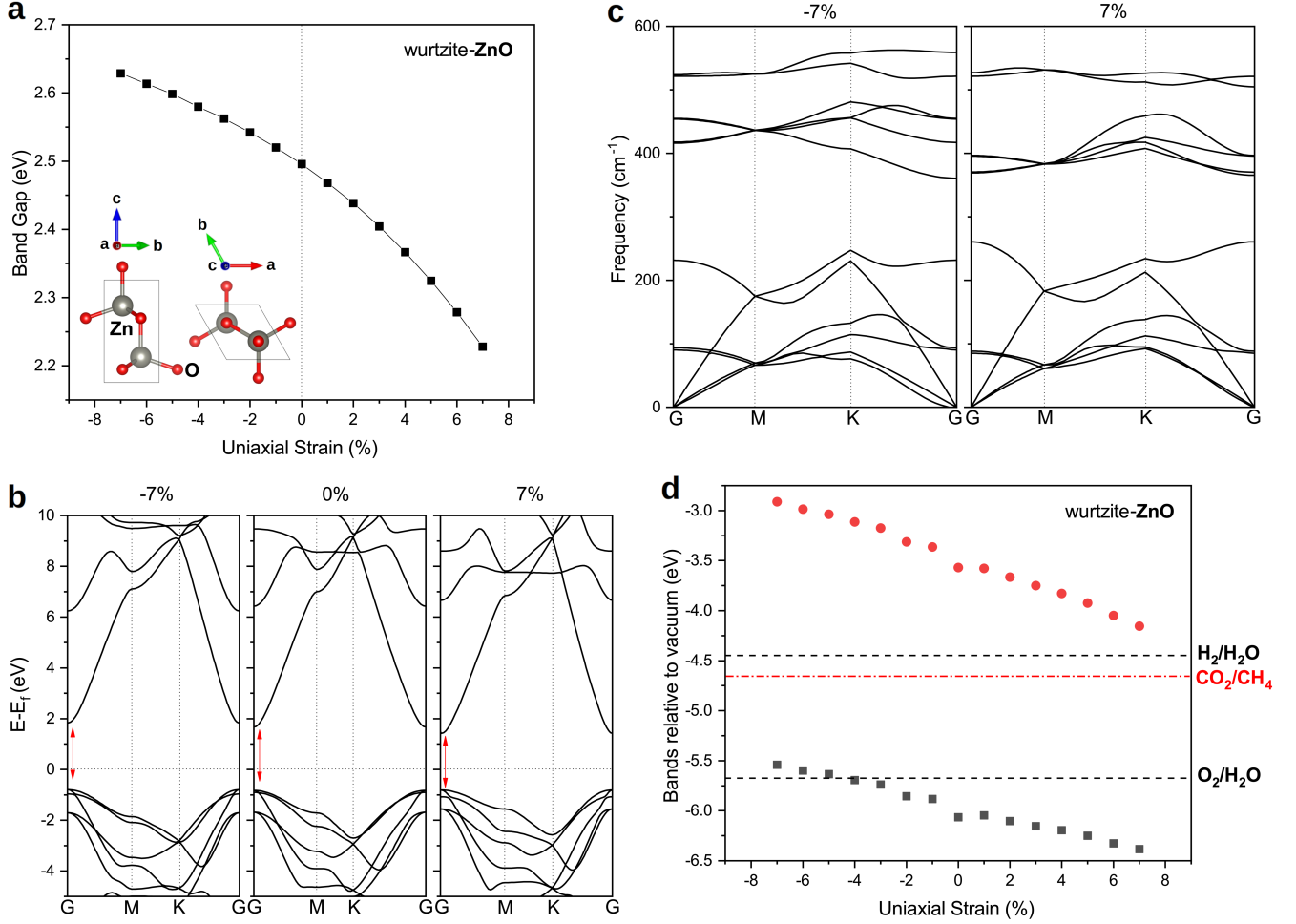


FIG. 6. First-principles analysis of the optoelectronic, vibrational, and band alignment properties of wurtzite ZnO. **a** Band-gap variation induced by uniaxial strain. **b** Dependence of the electronic band structure on uniaxial strain and reciprocal space point. **c** Phonon frequencies estimated as a function of uniaxial strain and reciprocal space point. **d** Effect of uniaxial strain on the band alignments of the crystal as referred to the vacuum level. The VBT and CBB energy levels are represented with solid grey squares and red circles, respectively.

tivity drawbacks are posed by the compounds SeBr and PI₃ (Table II), which should neither be contemplated in the context of green hydrogen production applications. Notwithstanding such limitations, these water unsuited piezo-photocatalyst materials could turn out to be useful for catalyzing other green chemistry reactions not requiring of aqueous media (e.g., CO₂ reduction [36]) hence we cautiously keep them in our list of selected candidates.

In the second position of Table II, it appears the oxide perovskite KNbO₃ for which recently its great piezo-photocatalyst potential has been experimentally recognized [29, 30] and which according to our calculations possesses superior photocatalytic band structure properties than BaTiO₃ (i.e., a slightly smaller band gap and a larger α_n^{rev} coefficient). In the third and fourth positions, we find LaN and PtF₄, two materials that, to the best of our knowledge, have not been investigated thus far as potential water splitting photocatalysts in spite of their ap-

propriate band gap and large band alignments tunability. Both materials, however, contain scarce elements like La and Pt hence their main drawback may be the high costs associated with their production. Similar expense limitations may also affect the three chalcogenide compounds BiTeCl, MgTe and BiTeI appearing in the eighth, tenth and twelfth positions in Table II, respectively, since they contain the rare Earth element Te. Concerning these latter systems, it may be interesting to explore whether similar piezo-photocatalyst performances can be attained by means of chemical substitutions based on the more abundant chalcogenide species Se and S.

Interestingly, GaN, a well-known direct band-gap semiconductor extensively used in light-emitting applications, appears in the ninth position of our ranking. The photocatalytic activity of this material in water-splitting hydrogen production has been already assessed and seems to be quite promising [37, 38]. Since GaN is a well-known

piezoelectric and technologically relevant material, it is likely that its piezo-photocatalytic performance will be eventually assessed; however, to the best of our knowledge, this possibility has not been yet addressed in the scientific literature. On this regard, our high-throughput computational screening suggests that it could be also very opportune to consider the alike nitride LaN since this compound ranks in the third position of our candidate piezo-photocatalyst list and in terms of production costs seems to be comparable to GaN.

By overlooking the water soluble, high cost and already known piezo-photocatalytic compounds reported in Table II, we are left with the halide AgI and semiconductor SiC. These two materials are very well known from their use in numerous applications ranging from industry and electronics to energy conversion [39, 40], and they can be efficiently produced in different morphologies and large quantities. Therefore, even if the piezoelectric coefficients of AgI and SiC are noticeably smaller than those of, for instance, LaN and PtF₄, it appears to be worth assessing experimentally their actual water-splitting piezo-photocatalytic performances.

Finally, it is fair to acknowledge that due to the intrinsic limitations of computational DFT methods and the incompleteness of the targeted materials database, some potentially good piezo-photocatalysts may have escaped our high-throughput computational screening. An illustrative example of such fortuitous omissions is provided by hexagonal ZnO which, as we mentioned in a previous section, upon consideration of the band gap reported in the MP database failed to pass our second sieve condition of $1.23 \lesssim E_g \lesssim 3.0$ eV. Nevertheless, from previous experimental and computational first-principles studies it is actually known that ZnO is a promising water-splitting photocatalytic material and that its band gap is larger than 1.3 eV [11, 20–22, 41]. Thus, motivated by this fact and for completeness of the present work, we proceeded to explicitly estimate the η -induced band-gap and band-alignment variations in wurtzite ZnO.

Figure 6 shows the results of our first-principles calculations carried out for piezoelectric ZnO (hexagonal symmetry, space group $P6_3mc$). Strain-induced band lifting effects are fully taken into consideration in our first-principles DFT results. Under (compressive) tensile uniaxial strain the band gap of wurtzite ZnO remains direct and its magnitude steadily (increases) decreases (Fig.6a-b). The estimated E_g variation is less pronounced than found in SiC (Figs.4-5), although more regular. For example, the band-gap reduction (increase) attained at the highest tensile (compressive) strain considered here is of $\approx 11\%$ ($\approx 6\%$). At the same time, the vibrational stability of wurtzite ZnO is pertinently conserved under uniaxial strain (Fig.6c). The influence of uniaxial strain in the band alignments of ZnO (Fig.6d) is qualitatively very similar to that found in 4H-SiC (Fig.4d). In particular, both the VBT and CBB levels are shifted towards more (less) negative potential values under tensile (compressive) strains and the induced potential variations are

quasi linear. The $dV/d\eta$ values estimated for wurtzite ZnO, however, are roughly two times smaller than those found in 4H-SiC. Interestingly, according to our calculations the VBT and CBB positions in unstrained ZnO are already quite optimal for driving the water splitting reactions hence very small structural distortions should be enough to optimally adjust its piezo-photocatalyst performance.

CONCLUSIONS

We have presented a first-principles high-throughput screening of potential bulk piezo-photocatalytic materials able to accelerate the production of green hydrogen from water under sunlight when exposed to ultrasound waves and/or mechanical actuation. Our computational sieve relies on the DFT information found in the Materials Project database, which comprises about 1,000 bulk piezoelectrics, and an easy-to-compute bulk material descriptor deduced from a simple “piezoelectric plate capacitor” electrostatic model. In short, ideal piezo-photocatalysts should simultaneously exhibit large piezoelectric stress coefficients and small dielectric constants, two qualities that typically oppose each other, besides reasonable band gaps and VBT and CBB energy levels in the unstrained state. Already known good piezo-photocatalysts were retrieved by our computational searches (i.e., KNbO₃ and BaTiO₃) while some other compounds previously overlooked in the context of photocatalysis were also identified as very promising. Specifically, it was found that, in terms of strain-driven band-alignment tunability, the piezo-photocatalytic water splitting ability of the nitrides LaN and GaN, halides PtF₄ and AgI, chalcogenides BiTeCl, BiTeI and MgTe, and semiconductor SiC may be comparable to those of BaTiO₃ and ZnO. Other potential piezo-photocatalysts like bulk KIO₃ and PI₃ were also recognized in spite of their inappropriateness to work in aqueous environments (hence in practice are not suitable for water-splitting photocatalytic applications). The introduced piezo-photocatalyst screening approach is general and can be also applied to other important families of materials not considered in this study (e.g., two-dimensional compounds and solid solutions). Therefore, the present computational work advances knowledge in the field of state-of-the-art photocatalytic materials and is expected to motivate original and prolific experimental investigations in the context of sustainable hydrogen production driven by sunlight.

METHODS

First-principles calculations. First-principles calculations based on density functional theory (DFT) [26–28] were performed to simulate and analyze the influence of uniaxial strain, η , on the optoelectronic, vibrational

and band alignment properties of piezo-photocatalytic materials. The PBEsol functional [33] was used as it is implemented in the VASP software package [26]. We employed the “projector augmented wave” method to represent the ionic cores [42] by considering the most relevant electrons of each atomic species as valence. Wave functions were represented in a plane-wave basis truncated at 800 eV. For integrations within the Brillouin zone (BZ) of all materials we employed Monkhorst-Pack \mathbf{k} -point grids [43] of spacing $2\pi \times 0.01 \text{ \AA}^{-1}$. Uniaxially strained bulk geometry relaxations were performed with a conjugate-gradient algorithm that allowed for volume variations while imposing the structural constraints defining uniaxial strain [12]. In our simulations, uniaxial strain is defined as $\eta = (c - c_0)/c_0$, where c_0 represents the length of the strained lattice vector in the absence of any stress. Positive η values are considered tensile uniaxial strains and $\eta < 0$ compressive. Periodic boundary conditions were applied along the three directions defined by the lattice vectors hence possible surface effects were completely neglected in the bulk simulations (not so in the slab simulations, see below). The relaxations were halted when the forces acting on the atoms were all below $0.005 \text{ eV}\cdot\text{\AA}^{-1}$. By using these technical parameters we obtained zero-temperature energies that were converged to within 0.5 meV per formula unit. Uniaxial strain conditions were simulated at $\Delta\eta = 1\%$ intervals. In order to estimate accurate dielectric, piezoelectric and band gap properties, we employed the range-separated hybrid HSE06 exchange-correlation functional [34] to perform single-point calculations on the equilibrium geometries determined at the PBEsol level [44].

To estimate phonon frequencies we employed the “small-displacement” approach [45], in which the force-constant matrix of the crystal is calculated in real space by considering the proportionality between the atomic displacements and forces when the former are sufficiently small (in the present study this condition was satisfied for atomic displacements of 0.02 \AA). Large supercells containing hundreds of atoms were employed to guarantee that the elements of the force-constant matrix presented practically negligible values at the largest atomic separations. The computation of the nonlocal parts of the pseudopotential contributions were performed in reciprocal space in order to maximise the numerical accuracy of the computed forces. Once a force-constant matrix was determined, we Fourier transformed it to obtain the phonon frequencies for any arbitrary \mathbf{k} -point in the first BZ. This latter step was performed with the PHONOPY code [46], in which the translational invariance of the system was exploited to ensure that the three acoustic branches were exactly zero at the Γ point. Central differences for the atomic forces, that is, both positive and negative atomic displacements, were considered.

To calculate accurate band alignments we followed the work done by Moses and co-workers on binary semiconductors [47]. Briefly, both bulk and slab calculations were performed from which the alignment of

the electrostatic potential within the semiconductor material could be obtained relative to the vacuum level. From the slab calculations, the difference between the average electrostatic potential within the semiconductor material and in vacuum was obtained. From the bulk calculations, the band structure shifts relative to the average electrostatic potential were determined. These calculations were performed at each η point and involved the estimation of macroscopic and planar average potentials. The planar potential was computed by averaging potential values within a well defined plane (for instance, perpendicular to the surface of the slab), and the macroscopic potential was obtained by taking averages of the planar potential over distances of one unit cell along the chosen direction [48, 49]. The slab systems were thick enough to ensure that the electron density in the center of the slab was practically equal to that in the bulk material. We found that 1.2–1.8 nm thick semiconductor slabs accompanied by similarly large portions of vacuum provided sufficiently well converged results for the electrostatic potentials. Band alignments were systematically estimated at the geometrical center of the slabs. A standard hydrogen passivation scheme [50] was employed in the geometry relaxations of the wurtzite ZnO slabs in order to appropriately determine the relevant macroscopic and planar average potential levels (Supplementary Fig.3).

High-throughput screening. The high-throughput screening of potential piezo-photocatalyst was performed using the Matminer package [51]. A pre-existing dataset containing about 1,000 piezoelectric materials was loaded from the Materials Project database [23]. Based on our PPC model, the parameters needed for the high-throughput screening were the thickness (c), dielectric constant (ϵ) and piezoelectric constant (e_{33}) of each considered compound (Results section). The piezoelectric constants of such materials were retrieved from the piezoelectric tensors provided in the same dataset, and their thicknesses were approximated by the mean average of the three corresponding lattice parameters. The value of the dielectric constants and energy band gaps (E_g) were acquired from the Materials Project (MP) database via the corresponding materials mp-ID’s; compounds for which the dielectric properties were not reported in the MP database were dropped from our high-throughput screening. Therefore, it is possible that few piezoelectric materials with potentially high piezo-photocatalytic tunability were overlooked in our analysis.

DATA AVAILABILITY

The data that support the findings of this study are available from authors Z.L. and C.C. upon reasonable request.

- [1] International Energy Agency (2019). The future of hydrogen, IEA. Paris <https://www.iea.org/reports/the-future-of-hydrogen>
- [2] Idriss, H. Hydrogen production from water: past and present. *Curr. Opin. Chem. Eng.* **29**, 74 (2020).
- [3] Kudo, A. & Miseki, Y. Heterogeneous photocatalyst materials for water splitting. *Chem. Soc. Rev.* **38**, 253 (2009).
- [4] Chen, S., Takata, T. & Domen, K. Particulate photocatalysts for overall water splitting. *Nat. Rev. Mater.* **2**, 17050 (2017).
- [5] Asahi, R., Morikawa, T., Ohwaki, T., Aoki, K. & Taga, Y. Visible-light photocatalysis in nitrogen-doped titanium oxides. *Science* **293**, 269 (2001).
- [6] Mofarah, S. S., *et al.*, Coordination polymer to atomically thin, holey, metal-oxide nanosheets for tuning band alignment. *Adv. Mater.* **31**, 1905288 (2019).
- [7] Bahmanrokh, G., Cazorla, C., Mofarah, S. S., Shahmiri, R., Yao, Y., Ismail, I., Chen, W.-F., Koshy, P. & Sorrell, C. C. Band gap engineering of Ce-doped anatase TiO₂ through solid solubility mechanisms and new defect equilibria formalism. *Nanoscale* **12**, 4916 (2020).
- [8] Xu, Y., Mofarah, S. S., Mehmood, R., Cazorla, C., Koshy, P. & Sorrell, C. C. Design strategies for ceria nanomaterials: untangling key mechanistic concepts. *Mater. Horiz.* **8**, 102 (2021).
- [9] Park, H., Kim, H.-I., Moon, G.-H. & Wonyong, C. Photoinduced charge transfer processes in solar photocatalysis based on modified TiO₂. *Energy Environ. Sci.* **9**, 411 (2016).
- [10] Takanabe, K. Photocatalytic water splitting: Quantitative approaches toward photocatalyst by design. *ACS Catal.* **7**, 8006 (2017).
- [11] Liu, Z., Menéndez, C., Shenoy, J., Hart, J. N., Sorrell, C. C. & Cazorla, C. Strain engineering of oxide thin films for photocatalytic applications. *Nano Energy* **72**, 104732 (2020).
- [12] Liu, Z., Wang, B. & Cazorla, C. Mechanical and electronic properties of CeO₂ under uniaxial tensile loading: A DFT study. *Materialia* **15**, 101050 (2021).
- [13] Zhang, L., Chen, J., Fan, L., Diéguez, O., Cao, J., Pan, Z., Wang, Y., Wang, J., Kim, M., Deng, S., Wang, J., Wang, H., Deng, J., Yu, R., Scott, J. F. & Xing, X. Giant polarization in super-tetragonal thin films through interphase strain. *Science* **361**, 494 (2019).
- [14] Hu, S., Wang, Y., Cazorla, C. & Seidel, J. Strain-enhanced oxygen dynamics and redox reversibility in topotactic SrCoO_{3-δ} ($0 \leq \delta \leq 0.5$). *Chem. Mater.* **29**, 708 (2017).
- [15] Dang, C., Chou, J.-P., Dai, B., Chou, C.-T., Yang, Y., Fan, R., Lin, W., Meng, F., Hu, A., Zhu, J., Han, J., Minor, A. M., Li, J. & Lu, Y. Achieving large uniform tensile elasticity in microfabricated diamond. *Science* **371**, 76 (2021).
- [16] Phan, H.-P., Nguyen, T.-K., Dinh, T., Ina, G., Kermany, A. R., Qamar, A., Han, J., Namazu, T., Maeda, R., Dao, D. V. & Nguyen, N.-T. Ultra-high strain in epitaxial silicon carbide nanostructures utilizing residual stress amplification. *Appl. Phys. Lett.* **110**, 141906 (2017).
- [17] Blagov, A. E., Kovalchuk, M. V., Pisarevskii, Y. V. & Prosekov, P. A. Control of the crystal lattice strain gradient caused by low-frequency ultrasound. *Crystallogr. Rep.* **53**, 379 (2008).
- [18] Truell, R., Elbaum, C. & Chick, B. B. Ultrasonic methods in solid state physics. New York, Academic Press (1969).
- [19] Wu, W. & Wang, Z. Piezotronics and piezo-phototronics for adaptive electronics and optoelectronics. *Nat. Rev. Mater.* **1**, 16031 (2016).
- [20] Tu, S., Guo, Y., Zhang, Y., Hu, C., Zhang, T., Ma, T. & Huang, H. Piezocatalysis and piezo-photocatalysis: Catalysts classification and modification strategy, reaction mechanism, and practical application. *Adv. Funct. Mater.* **30**, 2005158 (2020).
- [21] Liang, Z., Yan, C.-F., Rtimi, S. & Bandara, J. Piezoelectric materials for catalytic/photocatalytic removal of pollutants: Recent advances and outlook. *Appl. Catal. B: Environ.* **241**, 256 (2019).
- [22] Sakthivel, T., Venugopal, G., Durairaj, A., Vasanthkumar, S. & Huang, X. Utilization of the internal electric field in semiconductor photocatalysis: A short review. *J. Ind. Eng. Chem.* **72**, 18 (2019).
- [23] de Jong, M., Chen, W., Geerlings, H., Asta, M. & Persson, K. A. A database to enable discovery and design of piezoelectric materials. *Sci. Data* **2**, 150053 (2015).
- [24] Dash, S., Pradhan, D. K., Kumari, S., Rahaman, R. M., Cazorla, C., Brajesh, K., Kumar, A., Thomas, R., Rack, P. D. & Pradhan, D. K. Enhanced ferroelectric and piezoelectric properties of BCT-BZT at the morphotropic phase boundary driven by the coexistence of phases with different symmetries. *Phys. Rev. B* **104**, 224105 (2021).
- [25] Cazorla, C. & Stengel, M. Electrostatic engineering of strained ferroelectric perovskites from first principles. *Phys. Rev. B* **92**, 214108 (2015).
- [26] Kresse, G. & Fürthmüller, J. Efficient iterative schemes for ab initio total-energy calculations using a plane-wave basis set. *Phys. Rev. B* **54**, 11169 (1996).
- [27] Cazorla, C. The role of density functional theory methods in the prediction of nanostructured gas-adsorbent materials. *Coord. Chem. Rev.* **300**, 142 (2015).
- [28] Cazorla, C. & Boronat, B. Simulation and understanding of atomic and molecular quantum crystals. *Rev. Mod. Phys.* **89**, 035003 (2017).
- [29] Yu, D., Liu, Z., Zhang, J., Li, S., Zhao, Z., Zhu, L., Liu, W., Lin, Y., Liu, H. & Zhang, Z. Enhanced catalytic performance by multi-field coupling in KNbO₃ nanostructures: Piezo-photocatalytic and ferro-photoelectrochemical effects. *Nano Energy* **58**, 695 (2019).
- [30] Zhang, Y., Shen, G., Sheng, C., Zhang, F. & Fan, W. The effect of piezo-photocatalysis on enhancing the charge carrier separation in BaTiO₃/KNbO₃ heterostructure photocatalyst. *Appl. Surf. Sci.* **562**, 150164 (2021).
- [31] Moustakas, T. D. & Paelella, R. Optoelectronic device physics and technology of nitride semiconductors from the UV to the terahertz. *Rep. Prog. Phys.* **80**, 106501 (2017).
- [32] J. P. Perdew. Density functional theory and the band gap problem. *Int. J. Quantum Chem.* **19**, 497 (1986).
- [33] Perdew, J. P., Ruzsinszky, A., Csonka, G. I., Vydrov, O. A., Scuseria, G. E., Constantin, L. A., Zhou, X. & Burke, K. Restoring the density-gradient expansion for

- exchange in solids and surfaces. *Phys. Rev. Lett.* **100**, 136406 (2008).
- [34] Krukau, A. V., Vydrov, O. A., Izmaylov, A. F. & Scuse-
ria, G. E. Influence of the exchange screening param-
eter on the performance of screened hybrid functionals. *J.*
Chem. Phys. **125**, 224106 (2006).
- [35] Park, J.-S. Comparison study of exchange-correlation
functionals on prediction of ground states and structural
properties. *Curr. Appl. Phys.* **22**, 61 (2021).
- [36] Jiang, C., Nichols, A. W., Walzer, J. F. & Machan, C.
W. Electrochemical CO₂ reduction in a continuous non-
aqueous flow cell with [Ni(cyclam)]²⁺. *Inorg. Chem.* **59**,
1883 (2020).
- [37] Kida, T., Minami, Y., Guan, G., Nagano, N., Akiyama,
M. & Yoshida, A. Photocatalytic activity of gallium nit-
ride for producing hydrogen from water under light ir-
radiation. *J. Mater. Sci.* **41**, 3527 (2006).
- [38] Shimosako, N. & Sakama, H. Quantum efficiency of pho-
tocatalytic activity by GaN films. *AIP Adv.* **11**, 025019
(2021).
- [39] She, X., Huang, A. Q., Lucía, O. & Ozpineci, B. Review
of silicon carbide power devices and their applications.
IEEE Trans. Indust. Electr. **64**, 8193 (2017).
- [40] Aznar, A., Lloveras, P., Romanini, M., Barrio, M.,
Tamarit, J.-L., Cazorla, C., Errandonea, D., Mathur, N.
D., Planes, A., Moya, X. & Mañosa, Ll. Giant barocaloric
effects over a wide temperature range in superionic con-
ductor AgI. *Nat. Commun.* **8**, 1851 (2017).
- [41] Choi, H.-J., Jang, W., Mohanty, B. C., Jung, Y.S., Soon,
A. & Cho, Y.-S. Origin of prestress-driven optical modu-
lations of flexible ZnO thin films processed in stretching
mode. *J. Phys. Chem. Lett.* **9**, 5934 (2018).
- [42] Blöchl P. E. Projector augmented-wave method. *Phys.*
Rev. B **50**, 17953 (1994).
- [43] Monkhorst, H. J. & Pack, J. D. Special points for
Brillouin-zone integrations. *Phys. Rev. B* **13**, 5188
(1976).
- [44] Shenoy, J., Hart, J. N., Grau-Crespo, R., Allan, N. L.
& Cazorla, C. Mixing thermodynamics and photocat-
alytic properties of GaP-ZnS solid solutions. *Adv. Theory*
Simul. **2**, 1800146 (2019).
- [45] Alfè, D. PHON: A program to calculate phonons using
the small displacement method. *Comp. Phys. Commun.*
180, 2622 (2009).
- [46] Togo, A. & Tanaka, I. First principles phonon calcula-
tions in materials science. *Scr. Mater.* **108**, 1 (2015).
- [47] Moses, P. G., Miao, M., Yan, Q., & Van de Walle, C. G.
Hybrid functional investigations of band gaps and band
alignments for AlN, GaN, InN, and InGaN. *J. Chem.*
Phys. **134**, 084703 (2011).
- [48] Baldereschi, A., Baroni, S. & Resta, R. Band offsets
in lattice-matched heterojunctions: A model and first-
principles calculations for GaAs/AlAs. *Phys. Rev. Lett.*
61, 734 (1988).
- [49] Cazorla, C. & Stengel, M. First-principles modeling of
Pt/LaAlO₃/SrTiO₃ capacitors under an external bias po-
tential. *Phys. Rev. B* **85**, 075426 (2012).
- [50] Shiraishi, K. A new slab model approach for electronic
structure calculation of polar semiconductor surface. *J.*
Phys. Soc. Jpn. **59**, 3455 (1990).
- [51] Ward, L., *et al.* Matminer: An open source toolkit for
materials data mining. *Comput. Mater. Sci.* **152**, 60
(2018).

ACKNOWLEDGEMENTS

C.C. acknowledges support from the Spanish Min-
istry of Science, Innovation and Universities under the
“Ramón y Cajal” fellowship RYC2018-024947-I. Z.L. and
B.W. acknowledge support from the National Natu-
ral Science Foundation of China (12002402, 11832019),
the NSFC original exploration project (12150001), the
Project of Nuclear Power Technology Innovation Center
of Science Technology and Industry for National Defense
(HDLXZX-2021-HD-035), and the Guangdong Inter-
national Science and Technology Cooperation Program
(2020A0505020005). D.C. acknowledges support from
the Australian Research Council Projects (DP210100879,
LP190100829).

AUTHOR CONTRIBUTIONS

Z.L. and C.C. conceived the study and planned
the research. C.C. proposed the electrostatic mod-
elling of piezo-photocatalyst materials. Z.L. performed
the high-throughput computational screening of piezo-
photocatalysts based on the Materials Project database.
Z.L. and C.C. performed the supplementary and valida-
tion first-principles calculations and analysed the results
along with the rest of co-authors. The manuscript was
written by C.C. with substantial input from the rest of
co-authors.

ADDITIONAL INFORMATION

Supplementary information is available in the online
version of the paper.

COMPETING FINANCIAL INTERESTS

The authors declare no competing financial interests.